

# Application of hyperspectral remote sensing for environment monitoring in mining areas

Bing Zhang · Di Wu · Li Zhang · Quanjun Jiao ·  
Qingting Li

Received: 13 April 2010 / Accepted: 9 May 2011 / Published online: 26 May 2011  
© Springer-Verlag 2011

**Abstract** Environmental problems caused by extraction of minerals have long been a focus on environmental earth sciences. Vegetation growing conditions are an indirect indicator of the environmental problem in mining areas. A growing number of studies in recent years made substantial efforts to better utilize remote sensing for dynamic monitoring of vegetation growth conditions and the environment in mining areas. In this article, airborne and satellite hyperspectral remote sensing data—HyMap and Hyperion images are used in the Mount Lyell mining area in Australia and Dexing copper mining area in China, respectively. Based on the analyses of biogeochemical effect of dominant minerals, the vegetation spectrum and vegetation indices, two hyperspectral indices: vegetation inferiority index (VII) and water absorption disrelated index (WDI) are employed to monitor the environment in the mining area. Experimental results indicate that VII can effectively distinguish the stressed and unstressed vegetation growth situation in mining areas. The sensitivity of VII to the vegetation growth condition is shown to be superior to the traditional vegetation index—NDVI. The other index, WDI, is capable of informing whether the target vegetation is affected by a certain mineral. It is an important index that can effectively distinguish the

hematite areas that are covered with sparse vegetation. The successful applications of VII and WDI show that hyperspectral remote sensing provides a good method to effectively monitor and evaluate the vegetation and its ecological environment in mining areas.

**Keywords** Environment monitoring · Spectral analysis · Vegetation index · Hyperspectral remote sensing · Mining

## Introduction

Mining activities usually cause serious heavy metal pollution in soil and water. The weathering of mullock and mining tailings helps transportation of the heavy metal in polluted areas into soil, rivers, and groundwater, resulting in damage to the ecosystem in surrounding areas (Shi et al. 2002). The presence of heavy metal elements in minerals can lead to vegetation variety and impact vegetation growth. Monitoring vegetation growth is important, especially, in mining areas because vegetation indirectly reflects its growing environment. The traditional method of vegetation growth monitoring, field investigation has the disadvantage of cost-consuming, time-consuming, and labor-consuming, and cannot provide accurate information for large spatial area. The application of remote sensing data in monitoring and effective evaluation of vegetation and its growing environment in mining areas can provide prompt information about vegetation growth and solid scientific background for policy makers in environmental control in those areas.

The pollution in the ecosystem and the damage to vegetation can be effectively diagnosed and monitored by remote sensing technology (Xu et al. 2003). The hyperspectral data provides us an effective tool for monitoring

---

B. Zhang (✉) · D. Wu · L. Zhang · Q. Jiao · Q. Li  
Center for Earth Observation and Digital Earth,  
Chinese Academy of Sciences, No. 9 Dengzhuang South Road,  
Haidian, Beijing 100094, People's Republic of China  
e-mail: zb@ceode.ac.cn

D. Wu  
Graduate University of Chinese Academy of Sciences,  
19A Yuquanlu, Beijing 100049, People's Republic of China  
e-mail: dwu@ceode.ac.cn

plant species (Davison et al. 1999), vegetation growth condition (Noland et al. 2003; Lévesque and King 2003; Li et al. 2008), bio-chemical information (Asner et al. 1998; Curran 1994; Lewis et al. 2001; Sampson et al. 2003; Zarco-Tejada et al. 2004a and b), and mining environments (Gan et al. 2004). Various technologies based on airborne and satellite imagery have been used to monitor vegetation growth conditions, including the vegetation indices (VI), red edge effect, spectral absorption feature analysis, spectral blended analysis, wavelet transformation, and neural networks (Ustin et al. 1999; Li et al. 2005). The hyperspectral vegetation indices are widely used in analyses of lignin and nitrogen element content (Serrano et al. 2002), water content (Sims and Gamon 2003), leaf area index (Haboudane et al. 2004; Ludwig et al. 2007; Houborg et al. 2007), chlorophyll content (Hu et al. 2004; Zhang et al. 2008; Darvishzadeh et al. 2008), and have also been frequently used in monitoring vegetation and the environment (Broge and Mortensen 2002). In recent years, many efforts have been devoted to the biogeochemical effects monitoring and vegetation growing environment evaluation via remote sensing: Garty et al. (2001) explored the connection between wave spectrum of fruticose lichen and the degree of air pollution; Schuerger et al. (2003) detected the zinc effect on grass and chlorophyll concentrations by hyperspectral and fluorescence data; Kooistra et al. (2004) attempted to determine the relationship between reflectivity feature of field vegetation and heavy metal pollution in flood plains; Rosso et al. (2005) and Li et al. (2005) investigated the heavy metal pollution in soil and biological effect and wave spectral features of Virginia *Salicornia europaea* coerced by heavy metal and oil–gas pollution, as well as the investigation and application of heavy metal pollution in soil; Dunagan et al. (2007) studied the effect of Hg polluted soil onto visible infrared spectrum of spinach that grows in the soil and Gallagher et al. (2008) investigated the effect of enriched heavy metal in soil onto gray birch productivity.

Vegetation indices, which are normally based on satellite observation in the red and near-infrared wavebands, are widely employed as measures of green vegetation density and the absorption rate of photosynthetic solar radiation. However, these vegetation indices have limitations. For instance, the most widely used normalized difference vegetation index (NDVI) is easy saturation over dense vegetation areas and sensitive to the canopy backgrounds of the vegetation (Huete and Liu 1994; Leprieur et al. 2000; Jiang et al. 2006). In other words, NDVI is sensitive to the fraction of vegetation coverage, as well as low chlorophyll concentrations (Yoder and Waring 1994). However, it is not sensitive to higher chlorophyll concentrations or to rate of photosynthesis for large vegetation coverage (Gitelson et al. 1996). While a number of alternative vegetation

indices based on the same two spectral bands has been developed since NDVI, most indices have the aim of reducing the sensitivity of the index to extraneous factors such as soil background or the atmosphere (Steven et al. 2003). However, stressed vegetation, which indicates the environment deterioration in the mining area, cannot be distinguished from the environmental background with a wide range of chlorophyll-a concentration.

This paper has two objectives: (1) how to use an effective vegetation index, based on both airborne and satellite hyperspectral images, to monitor the vegetation growth condition which could indirectly reflect the vegetation growing environment in the mining environmental stress area and (2) how to adopt a new hyperspectral index that is suitable to directly monitor the poor vegetation growth environments that are affected by a certain mineral in the mining area. Based on an analysis of the geochemical effects on vegetation in the mining area together with a detailed analysis of vegetation spectrum and vegetation indices, two spectral indices derived from hyperspectral data that are applicable to the evaluation of vegetation environment in the mining area were proposed. The intention of this paper was to develop tools for fast and quantitative monitoring of vegetation conditions in mining areas and effective evaluation of vegetation growing environment in mining areas.

## Materials and theory

### Study area and remote sensing data

The experiments were performed in the Mountain Lyell mining area in Tasmania and Dexing copper mining area, Jiangxi Province in China. Tasmania, located in the south of Australia, is the only island of Australia and is abundant in mineral resources. The largest reserve of mineral resources is found in its rugged western region. Mountain Lyell is in the Queenstown area in the west of Tasmania. It has abundant minerals such as copper, silver, and gold, which have been extracted since 1885, and produces large amounts of copper pyrite, quartz, hematite, and dolomite (Raymond 1996; Corbett 2001). Intensive exploitation for more than 100 years has inevitably brought negative effects on the ecosystem in this area, including a drop in the water level, land subsidence, soil acidification, decreased vegetation coverage, and a vulnerable ecological environment (Featherstone and O'Grady 1997; Stauber et al. 2000; Gault et al. 2005). Dexing copper mine is the largest open-cast mine in China and is the second largest in the world. It accounts for about 20% of total Chinese production with daily output capacity of more than 100,000 tons. The problems associated with mining are: the weathering of waste-rock piles

which produces a large quantity of acidic drainage, and the discharge from the ore-flotation plant, which produces large amounts of alkaline effluent with a high content of fine ore-tailing particles (Muller and Tang 1996).

This paper uses hyperspectral remote sensing data for the two test sites obtained in 2003 by the HyMap imaging spectrometer developed by Australian Integrated Spectronics and in 2009 by the Hyperion imaging spectrometer developed by NASA, respectively. HyMap and Hyperion both continuously cover the visible to short-wave infrared spectral regions (400–2,500 nm). HyMap has 128 wavebands, while Hyperion has 242 bands. The spectral resolution of HyMap is 10–20 nm with an instantaneous field (IFOV) view of 1–3 mrad and with viewing angles from 30 to 65°. On the other hand, Hyperion has a spectral resolution of 10 nm, IFOV of 0.043 mrad, crosstrack FOV of 0.63 mrad (Cocks et al. 1998; Pearlman et al. 2003). The airborne instrument of HyMap is equipped with navigation and location system, positioning and attitude parameters recording device, and a three-axis stabilized gyro platform. The manufacturer also developed the 6S-based special module for atmospheric correction of images. HyMap features a high signal-to-noise ratio (500:1), high-ground resolution (5–10 m), and fine spectral resolution, and has great potential in ground-object identification and environment monitoring. Hyperion, on the other hand, permits global quantitative temporal hyperspectral monitoring of earth surface processes, although its spatial resolution is coarser (30 m) compared with that of HyMap.

**Experiment and theory**

According to field investigations, vegetation health is negatively correlated with the distance of the vegetation from its closest mine. Therefore, plants far away from the mine grow better. Mismanagement of the mining area and gangue leads to great content of heavy metal elements in

soil near the mine. After the infiltration enters into soil, the heavy metal pollutants would have physical, chemical and biological reactions with soil components, which lead to soil acidification or basification, and the elution and seepage of soluble pollutants cause groundwater and surface water contamination. These pollutants could be absorbed by vegetation and engaged in a series of biogeochemical reactions, which can result in poor growth conditions of vegetation near the mine. The process of pollution changes the vegetation biochemical parameters and the corresponding spectrum, which enables us the extraction of vegetation spectral curve and analyzes its pollution information in the mining area. Li et al. (1996) measured the reflection spectrum of paddy rice leaf in soil under different acidification and suggested that the reflectance value at different wavebands varies with acidity: where reflectance at blue, green, and red wavebands increases as the pH value decreases, while the reflectance of near infrared decreases with decreased pH value (Fig. 1a). Similarly, the spectra which are extracted from the regions of dense and sparse vegetations in the HyMap imagery in the test site show that the reflectance for the dense vegetation (better growth conditions) is lower than that for sparse vegetation (poor growth conditions) at blue, green, and red wavebands, but higher in the near-infrared waveband (Fig. 1b).

Commonly, spectral indices of vegetation are established with reflectance at NIR and RED wavebands. The normalized difference vegetation index is originally defined as:

$$NDVI = (\rho_{NIR} - \rho_{RED}) / (\rho_{NIR} + \rho_{RED}) \times 100 \quad (1)$$

where,  $\rho_{NIR}$  and  $\rho_{RED}$  is the reflectance in near-infrared waveband and red waveband, respectively. Based on the spectral characteristics that were mentioned earlier as shown in Fig. 1, the visible and near-infrared waveband reflectance can be used to produce the effective index that measures the vegetation growing conditions. NIR is indicative wavebands that distinguish the different vegetation growing environments. The atmospheric effect in NIR

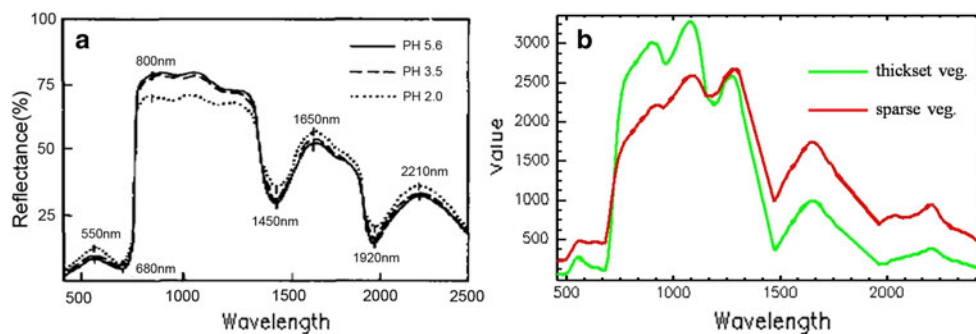


**Fig. 1** **a** The spectral response of rice leaves in different soil acidity (Li et al. 1996) and **b** the spectra for vegetation with different growth condition extracted from HyMap image. **a** indicated that the reflectance values at different wavebands (blue, green, red, and

near-infrared) varied with soil acidity, while the reflectance for the thick vegetation and sparse vegetation in (b) have the same trend with the reflectance as (a) shown

is small due to aerosol scattering and absorption. Gitelson et al. (1996) found that the bands of maximum sensitivity to chlorophyll-a concentration were around 520–630 nm (the green band) and also near 700 nm. The index GARI (using green and NIR bands) proposed in Gitelson's paper has wider dynamic range and on average at least five times more sensitive to chlorophyll-a concentration than NDVI (using red and NIR bands). Therefore, GREEN bands rather than RED bands (which are chosen by NDVI) are more suitable for monitoring vegetation growth conditions.

Of note, the Hymap and Hyperion images, which are used to establish the two indices on, are already the surface reflectance data (atmospheric correction implemented by the radiometric correction module that is developed by the manufacturer and integrated in the ENVI FLAASH module). The depths of the two-water absorption bands (near 960 and 1,100 nm) of vegetation that change with its growth conditions are highly related to each other. The indices (VII and WDI) that are introduced in the following sections are constructed utilizing the relationship mentioned earlier and the bands combination with the best sensitivity of chlorophyll-a concentration.

## Results and discussion

Using VII to monitor vegetation growth condition

Based on the aforementioned two theories, the integral of reflectivity at green peak and near-infrared is adopted to represent the growth condition of vegetation as hyperspectral images have relatively small spectral sample intervals and continuous coverage of the two wavebands, which is superior to other index with single green and near-infrared wavebands. This algorithm keeps the absorptive features at visible wavelength and the reflective characteristics at near-infrared waveband while it increases the contribution rate of growing environment to vegetation spectra, which avoids the ineffective measurement due to fast saturation of NDVI. The green bands from 497 to 635 nm and the near-infrared bands from 700 to 1,200 nm are chosen as they are sensitive to the concentration of chlorophyll-a for a wide range. The spectral integral approach is presented as follows:

$$\alpha = \int_{\lambda_1}^{\lambda_2} \rho(\lambda) d\lambda \quad \lambda \in [497, 635] \quad (2)$$

$$\beta = \int_{\lambda_3}^{\lambda_4} \rho(\lambda) d\lambda \quad \lambda \in [700, 1,200] \quad (3)$$

$$\Delta = \beta - \alpha \quad (4)$$

where,  $\alpha$  stands for the integral of reflectivity at green peak,  $\beta$  stands for the integral of reflectivity at near-infrared

portion,  $\Delta$  is the difference between integral values at near-infrared reflectivity and green peak reflectivity. Parameters  $\alpha$  and  $\beta$  in the formula are normalized respectively to make them on the same level as shown below:

$$N_\alpha = \alpha / \left( \sum \sum \alpha_{(x,y)} / (m \times n) \right) \quad (5)$$

$$N_\beta = \beta / \left( \sum \sum \beta_{(x,y)} / (m \times n) \right) \quad (6)$$

$$N_\Delta = \Delta / \left( \sum \sum \Delta_{(x,y)} / (m \times n) \right) \quad (7)$$

where,  $N_\alpha$ ,  $N_\beta$  and  $N_\Delta$  stand for the normalized values of the integral of reflectivity at the green peak, the near-infrared portion, and the normalized difference value, respectively. The subscript  $x$  and  $y$  identify the row and column of each pixel in the hyperspectral image, while  $m$  and  $n$  stand for the number of rows and columns of the study area. In the areas with poor vegetation growth condition or barren soil,  $N_\alpha$  will be higher,  $N_\beta$  will be lower, so  $N_\Delta$  will be reduced (Fig. 1). Areas with vegetation cover are masked by setting the threshold to the featured bands (represent the best contrast between spectra of different growth conditions, referred to the "continuum removal" algorithm (Clark and Roush 1984) of HyMap and Hyperion reflectivity images.

$N_\alpha$ ,  $N_\beta$ , and  $N_\Delta$  were calculated for each pixel in the vegetation area and generate a composite image (red band,  $N_\alpha$ ; blue band,  $N_\beta$  and green band,  $N_\Delta$ ). Therefore, red pixels are the areas where vegetation grows poorly and the cyan pixels have better vegetation growth as shown in Fig. 2. Figure 2 is part of the composite image in the mining area (Gormanston, east of Queenstown), where there was great environmental pressure and serious pollution. While the vegetation in this area had poor growth condition, this composite image can still highlight the

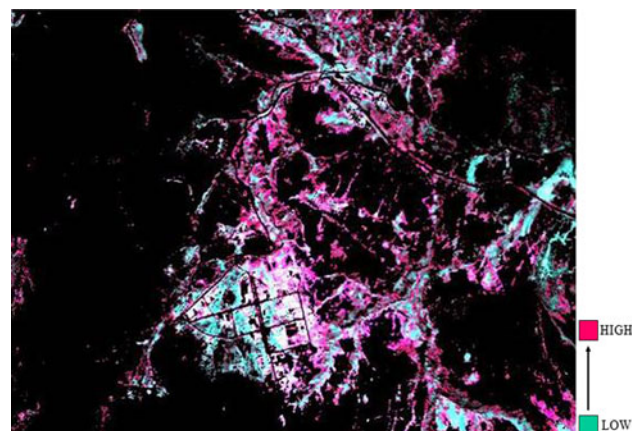
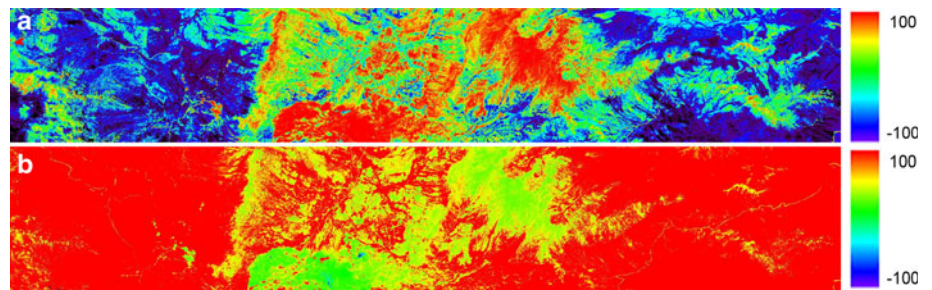


**Fig. 2** The composite image of  $N_\alpha$ ,  $N_\beta$  and  $N_\Delta$  in Gormanston (*High*: Bad growth conditions, *Low*: good growth conditions)



**Fig. 3** VII image (a) and NDVI (b) image derived from HyMap imagery over the study area in Mount Lyell mining area. VII effectively distinguish whether the growth of vegetation is good or bad in the mining area with environmental pressure that NDVI could not do



differences. Hence, it has a relatively high sensitivity to vegetation growth condition.

Therefore, the vegetation inferiority index (VII) is defined as follows:

$$VII = (N_{\alpha} - N_{\beta}) / (N_{\alpha} + N_{\beta}) \times 100 \quad (8)$$

For the areas with poor vegetation growth, if  $N_{\alpha}$  is relatively high and  $N_{\beta}$  is relatively low, then the VII index becomes larger. Figure 3a shows the VII index derived from the HyMap data over the study area. In the mining area, northwest and southeast of the study area, the vegetation obviously grew worse than in the north and south of the study area. Furthermore, VII could reflect the difference of the vegetation growth within the mining area and also show the influence scope of the mineral environment pollution. Figure 3b depicts the NDVI image derived from the HyMap imagery over the study area. Compared with Fig. 3a, the vegetation growth condition is not well reflected in NDVI image due to fast saturation of NDVI in the dense vegetation area. However, for the area with relatively poor growth, vegetation cannot be distinguished from the environmental background.

To further compare VII and NDVI, the vegetation area over the mining area was chosen to analyze the histograms. Figure 4a shows that the VII histogram after linear contrast stretch is extended fully between 0 and 255 and the images present a good contrast ratio, whereas a large portion of the NDVI values are clustered near the minimum and maximum values when the NDVI histogram is stretched (Fig. 4b), which is not optimal for the classification of vegetation growth condition.

In addition, Fig. 5 shows the VII and NDVI images using two reverse color look-up tables. It is clear that NDVI index indicates good growth conditions for most of the vegetation in the mining area, whereas the VII index clearly depicts the medium-to-poor gradient of vegetation growth conditions, which is in accordance with the fact. Compared with NDVI, VII index can better identify the difference in vegetation growth conditions. Hence, VII will have more advantages for indirectly reflecting vegetation growing environment in mining area.

This index is also applied to satellite hyperspectral images to test its applicability to satellite observation

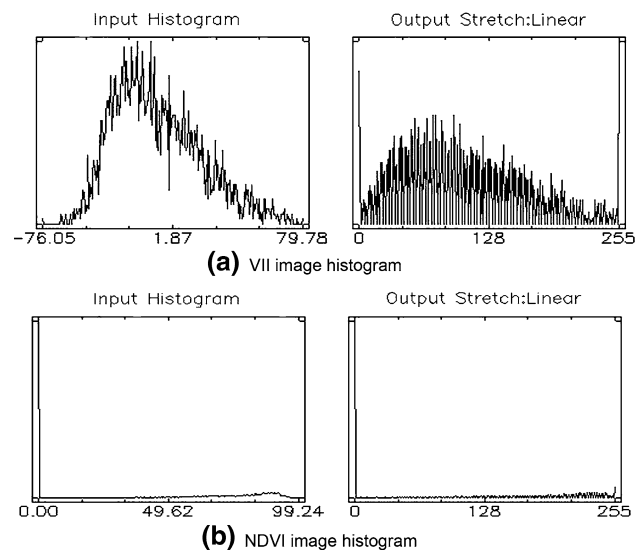


**Fig. 4** A Comparison of the stretched histograms of VII (a) and NDVI (b) over the vegetation areas

system. The VII index is calculated from the Hyperion images for the Dexing copper mining area in Jiangxi Province of China to analyze the spatial distribution of pollution in this area (Fig. 6). For vegetation areas surrounded by rivers and gangue, VII showed gradual transition from red to blue, indicating the relatively poor growth condition, which is consistent with the field investigation and previous literatures (Gan et al. 2004; Liu et al. 2004; Li 2006). This reinforces the conclusion showing that VII can indirectly reflect, to some extent, the polluted environment in mining areas through analyzing the vegetation growth condition.

#### The application of WDI on environment monitoring in mining areas

VII could only reflect whether the vegetation growing environment is good or bad in the mining area; however, it is not capable of identifying whether the vegetation growing environment is abundant in certain kinds of metal or heavy metal mineral. Therefore, it is necessary to develop a method that able to identify the minerals covered with vegetation to obtain accurate growth conditions of

**Fig. 5** Comparison of the color density slice images of VII (*left*) and NDVI (*right*) using two reverse color look-up tables

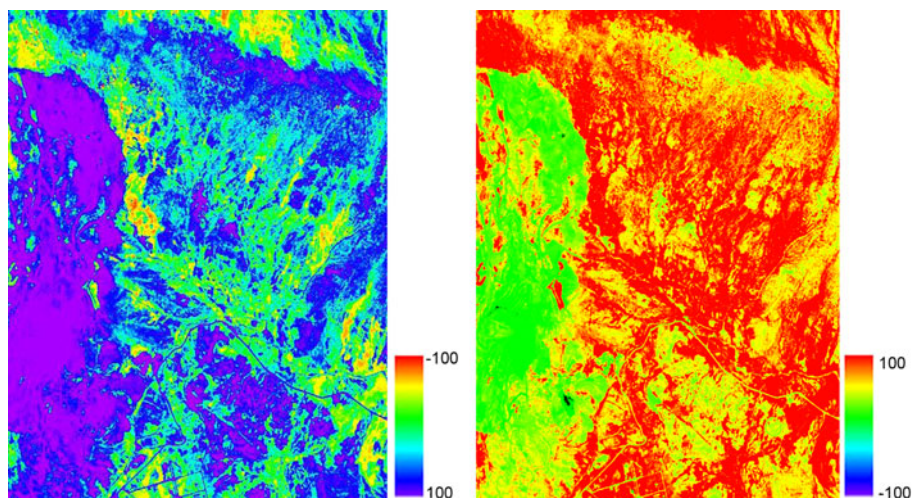
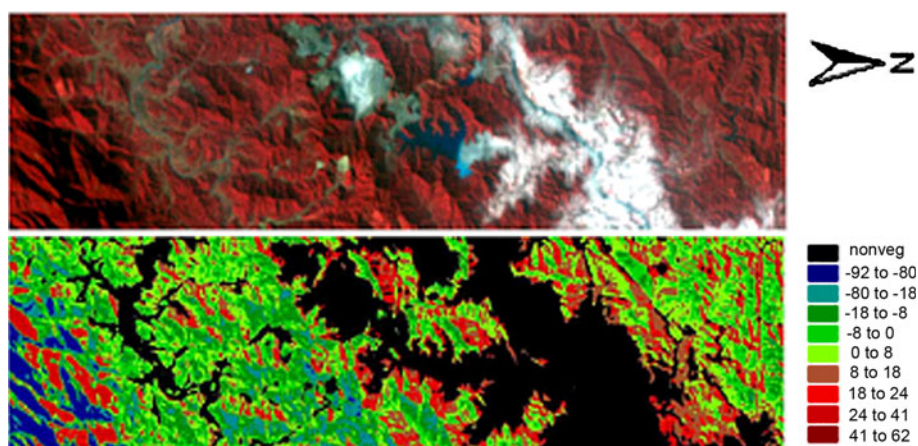


**Fig. 6** The VII index image (*b*) of the DEXING mining area derived from Hyperion data (*a*)



vegetation in the mining area. WDI is an important index that can effectively distinguish the exposed hematite area from a large amount of vegetation coverage, especially the hematite areas that are covered with sparse vegetation.

There are two weak water-vapor absorption belts for healthy vegetation near the infrared spectral bands at 0.968 and 1.181  $\mu\text{m}$  as shown in Fig. 7a. Two weak water-vapor absorption belts are both mainly formed by water content in green leaves; therefore, the changes of the two absorption valleys on vegetation spectra have similar trends. Analysis of leaf water absorption index (LWAI) (Fig. 8) derived from the two absorption valleys of green leaves on HyMap images shows that there is a high correlation between the two absorption valleys.

The spectrum (Fig. 7b) of iron ore shows that there is an absorption valley near 0.96  $\mu\text{m}$  on the spectrum of iron ore, but no 1.1  $\mu\text{m}$  absorption; thus the absorption valley depths at these two places have no correlation. The spectrum features of soil differ from those of iron ore and vegetation because there is no strong absorption near 0.96 and 1.1  $\mu\text{m}$ . For the vegetation areas with iron ore as the underlying surface, the difference of absorption occurs near 0.96 and

1.1  $\mu\text{m}$ . Therefore, the iron ore region can be detected by applying thresholds to uncorrelated wavelengths at water-vapor absorption belts at pixel level. The water absorption disrelated index (WDI) is designed as follows:

$$\text{WDI} = \frac{\sum \text{LWAI}_{1,181}}{\sum \text{LWAI}_{968}} \text{LWAI}_{968} - \text{LWAI}_{1,181} \quad (9)$$

where,  $\sum \text{LWAI}_{1,181}$  is the accumulated value for  $\text{LWAI}_{1,181}$  and  $\sum \text{LWAI}_{968}$  is the accumulated value for  $\text{LWAI}_{968}$  of the whole study area. The absorption feature was normalized based on the statistics on the two accumulated absorption features for the entire map. Due to the strong correlation of the two absorption features in the vegetation areas, the WDI in the region with non-mineral pollution should be close to zero. As the two absorption features of soil is zero, the WDI value for bare soil is also close to zero. However, the WDI value in bared iron ore areas and the vegetation area contaminated by iron ore is not zero. In this study, WDI is retrieved from the HyMap image and the threshold of 0.4 for WDI is applied. The areas with the WDI higher than 0.4 suggest that the depths of the two-water absorption valleys are not highly



**Fig. 7** **a** The water absorption spectral feature of green leaves and **b** the spectral signature of Jarosite mineral

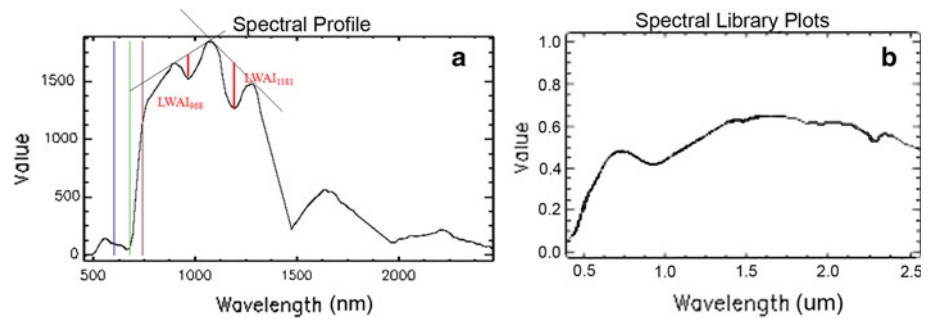
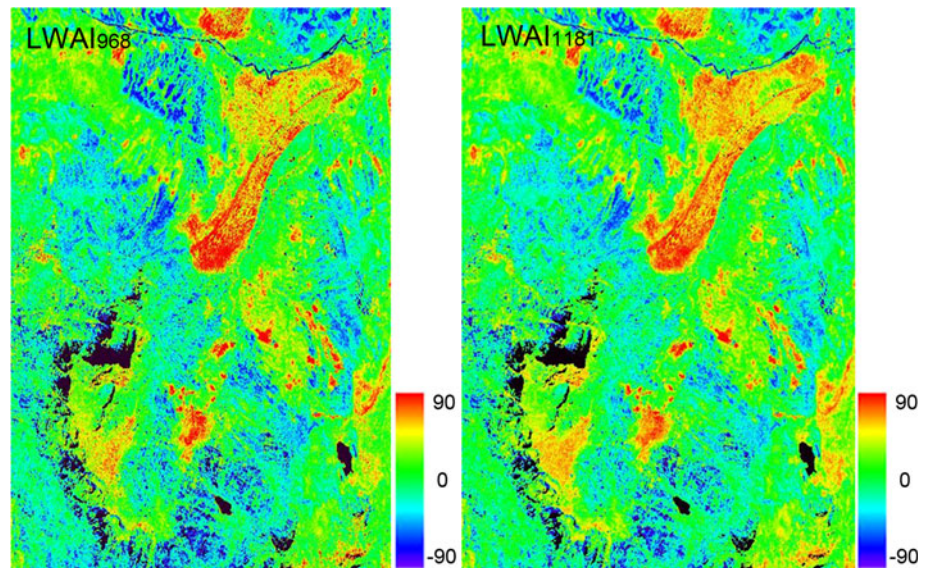


**Fig. 8** Two-water absorption spectral feature maps in non-iron ore areas with vegetation cover. It shows that there is high correlation between the two absorption valleys



correlated. The bare iron ore areas or the vegetation areas contaminated by iron ore are illustrated in the red portion of Fig. 9.

The reflectivity curve (Fig. 9c, middle) for a pixel in red is found to closely resemble the spectral feature of  $Fe_2O_3$  ore measured in the laboratory. It is well known that  $Fe_2O_3$  ore is stored at the bare surface of this mining area. According to Fig. 9, areas abundant in iron ore are also extracted in strip riverways on the right side of the iron ore areas, which is possibly formed by deposition of iron ore washed down by the stream. The bare areas around the riverway are identified as areas that are not abundant in iron minerals. There are large areas of bare rock-soil in the central part of the study area. The spectrum of the bare rock-soil area (Fig. 9c, upper) differs from the spectral signature of the iron ore area. From the above analysis, WDI can be used to distinguish bare iron ore areas from bare non-iron ore areas.

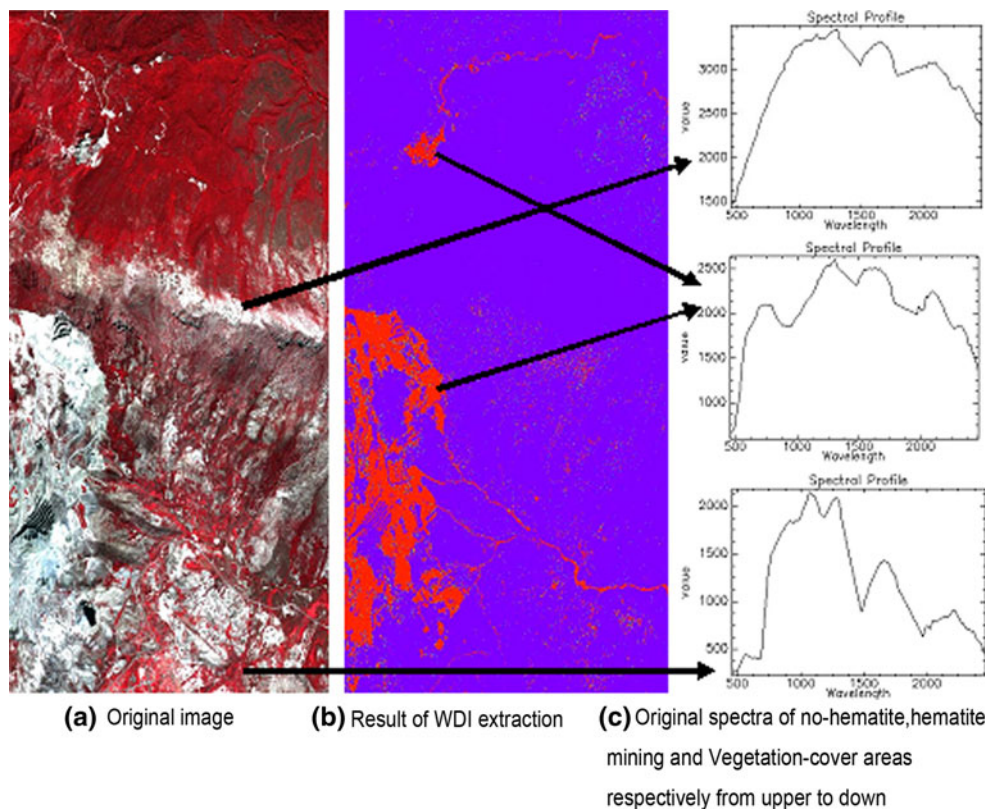
Except for the bare areas, the vegetation areas (either polluted or not polluted by iron ore) can also be identified by the WDI index. The comparison between the spectrum (Fig. 9c, lower) of the vegetation area containing iron ore and the spectrum of normal vegetation (Fig. 7a) reveals

that the vegetation area with iron ore has two absorption valleys at 0.96 and 1.1  $\mu m$  wavebands, which is different from the spectrum of normal vegetation. This is why WDI can identify the vegetation area with iron ore underneath.

**Conclusions**

Based on the analysis of the spectral features of the vegetation spectrums in the mining areas, two vegetation indices are introduced: VII and WDI. They are applied on HyMap and Hyperion hyperspectral data to monitor the vegetation growth condition and its growing environment in the Mount Lyell mining area and Dexing copper mine. Thus, the polluted environment caused by mining could be analyzed. The results showed that VII can effectively reflect the vegetation growth condition in mining areas and more sensitive than NDVI to the vegetation growth condition. Unlike other vegetation indices, VII mainly reflects the inferiority or environment stress of plants. VII value is high for vegetation growing on barren soil. Besides, VII can indirectly reflect the polluted environment in the vegetation areas. WDI can effectively identify the bare iron ore

**Fig. 9** WDI image derived from HyMap data. **a** is a part of the original HyMap image, **b** shows the result of WDI of **a**, the two-water absorption feature are not correlative or no high-correlation in the red part. **c** depicted the spectra of on-hematite, hematite mining and vegetation cover areas



area and the vegetation area contaminated by iron ore, which can be used for direct extraction of polluted regions in mining areas. These two vegetation indices derived from the hyperspectral remote sensing data can be used to monitor the vegetation coerce effect and growing environment. They are the effective indicators for a mining environment and can provide a policy basis for mining regulation. The successful use of these two indices proves that hyperspectral remote sensing has a strong potential in mining environment monitoring.

The VII index is not limited to any special type of mine. It is an index for normal monitoring of vegetation growth. In order to investigate vegetation growth status influenced by some specific heavy metals, further studies of the mineral spectral mechanism and vegetation physiological characteristics were required. Factors such as topography, moisture, fertilizer, and soil acidification in the mining areas should also be considered. The WDI index is intended to monitor the vegetation growing environment in iron ore areas, especially to identify the growing environment of iron ore in bare areas and areas with sparse vegetation. The WDI index is excellent to synchronously eliminate not only all vegetation, but also other mineral cover area, only determines the ferric oxide ( $\text{Fe}_2\text{O}_3$ ). A more hyperspectral index will be developed to identify other minerals such as copper in the future work. The identification of the growing

environment of dense vegetation can be achieved by the combination of more prior knowledge.

**Acknowledgments** This work was supported in part by the National Basic Research Program of China (973) under Grant No. 2009CB723902. The authors would like to acknowledge CSIRO Exploration and Mining, Australia for providing the HyMap datasets.

## References

- Asner GP, Braswell BH, Schimel DS, Wessman CA (1998) Ecological research needs from multiangle remote sensing data. *Remote Sens Environ* 63:155–165. doi:[10.1016/S0034-4257\(97\)00139-9](https://doi.org/10.1016/S0034-4257(97)00139-9)
- Broge NH, Mortensen JV (2002) Deriving green crop area index and canopy chlorophyll density of winter wheat from spectral reflectance data. *Remote Sens Environ* 81:45–57. doi:[10.1016/S0034-4257\(01\)00332-7](https://doi.org/10.1016/S0034-4257(01)00332-7)
- Clark RN, Roush TL (1984) Reflectance spectroscopy: quantitative analysis techniques for remote sensing applications. *J Geophys Res* 89:6329–6340. doi:[10.1029/JB089iB07p06329](https://doi.org/10.1029/JB089iB07p06329)
- Cocks T, Janssen R, Stewart A, Wilson I, Shields T (1998) The HyMap airborne hyperspectral sensor: the system, calibration and performance. In: 1st EARSEL Workshop on Imaging Spectroscopy. Zurich, Switzerland (Paris: ERSEL) 37–42
- Corbett KD (2001) New mapping and interpretations of the Mount Lyell Mining district, Tasmania: a large hybrid Cu–Au system with an exhalative Pb–Zn top. *Econ Geol* 96:1089–1122. doi:[10.2113/gsecongeo.96.5.1089](https://doi.org/10.2113/gsecongeo.96.5.1089)
- Curran PJ (1994) Imaging spectrometry. *Prog Phys Geog* 18(2): 247–266. doi:[10.1177/03091333](https://doi.org/10.1177/03091333)



- Darvishzadeh R, Skidmore AK, Schlerf M, Atzberger C, Corsi F, Cho MA (2008) LAI and chlorophyll estimation for heterogeneous grassland using hyperspectral measurements. *ISPRS J Photogramm* 63(4):409–426. doi:[10.1016/j.isprsjprs.2008.01.001](https://doi.org/10.1016/j.isprsjprs.2008.01.001)
- Davison D, Achal S, Mah S, Gauvin R, Kerr M, Tam A, Preiss S (1999) Determination of tree species and tree stem densities in northern Ontario forests using airborne CASI data. In: Proceedings of the Fourth International Airborne Conference and Exhibition, Ottawa, pp 187–196
- Dunagan SC, Gilmore MS, Varekamp JC (2007) Effects of mercury on visible/near-infrared reflectance spectra of mustard spinach plants (*Brassica rapa* P.). *Environ Pollut* 148(1):301–311. doi:[10.1016/j.envpol.2006.10.023](https://doi.org/10.1016/j.envpol.2006.10.023)
- Featherstone AM, O'Grady BV (1997) Removal of dissolved copper and iron at the freshwater-saltwater interface of an acid mine stream. *Mar Pollut Bull* 34(5):332–337. doi:[10.1016/S0025-326X\(96\)00089-6](https://doi.org/10.1016/S0025-326X(96)00089-6)
- Gallagher FJ, Pechmann I, Bogden JD, Grabosky J, Weis P (2008) Soil metal concentrations and productivity of *Betula populifolia* (gray birch) as measured by field spectrometry and incremental annual growth in an abandoned urban Brownfield in New Jersey. *Environ Pollut* 156(3):699–706. doi:[10.1016/j.envpol.2008.06.013](https://doi.org/10.1016/j.envpol.2008.06.013)
- Gan FP, Liu SW, Zhou Q (2004) Identification of mining pollution using hyperion data at Dexing copper mine in Jiangxi Province, China. *Earth Sci J China Univ Geosci* 29(1):119–126
- Garty J, Weissman L, Cohen Y, Karnieli A, Orlovsky L (2001) Transplanted lichens in and around the Mount Carmel National Park and the Haifa Bay industrial region in Israel, physiological and chemical responses. *Environ Res* 85(2):159–176. doi:[10.1006/enrs.2000.4222](https://doi.org/10.1006/enrs.2000.4222)
- Gault AG, Cooke DR, Townsend AT, Charnock JM, Polya DA (2005) Mechanisms of arsenic attenuation in acid mine drainage from Mount Bischoff, western Tasmania. *Sci Total Environ* 345:219–228. doi:[10.1016/j.scitotenv.2004.10.030](https://doi.org/10.1016/j.scitotenv.2004.10.030)
- Gitelson AA, Kaufman YJ, Merzlyak MN (1996) Use of a green channel in remote sensing of global vegetation from EOS-MODIS. *Remote Sens Environ* 58:289–298. doi:[10.1016/S0034-4257\(96\)00072-7](https://doi.org/10.1016/S0034-4257(96)00072-7)
- Haboudane D, Miller JR, Pattey E, Zarco-Tejada PJ, Strachan I (2004) Hyperspectral vegetation indices and novel algorithms for predicting green LAI of crop canopies: modeling and validation in the context of precision agriculture. *Remote Sens Environ* 90(3):337–352. doi:[10.1016/j.rse.2003.12.013](https://doi.org/10.1016/j.rse.2003.12.013)
- Houborg R, Soegaard H, Boegh E (2007) Combining vegetation index and model inversion methods for the extraction of key vegetation biophysical parameters using Terra and Aqua MODIS reflectance data. *Remote Sens Environ* 106:39–58. doi:[10.1016/j.rse.2006.07.016](https://doi.org/10.1016/j.rse.2006.07.016)
- Hu B, Qian S-E, Haboudane D, Miller JR, Hollinger AB, Tremblay N, Pattey E (2004) Retrieval of crop chlorophyll content and leaf area index from decompressed hyperspectral data: the effects of data compression. *Remote Sens Environ* 92:39–152. doi:[10.1016/j.rse.2004.05.009](https://doi.org/10.1016/j.rse.2004.05.009)
- Huete AR, Liu HQ (1994) An error and sensitivity analysis of the atmospheric- and soil-correcting variants of the NDVI for the MODIS-EOS. *IEEE T Geosci Remote* 32(4):897–905. doi:[10.1109/36.298018](https://doi.org/10.1109/36.298018)
- Jiang Z, Huete AR, Chen J, Chen Y, Li J, Yan G, Zhang X (2006) Analysis of NDVI and scaled difference vegetation index retrievals of vegetation fraction. *Remote Sens Environ* 101:366–378. doi:[10.1016/j.rse.2006.01.003](https://doi.org/10.1016/j.rse.2006.01.003)
- Kooistra L, Salas EAL, Clevers JGPW, Wehrens R, Leuven RSEW, Nienhuis PH, Buydens LMC (2004) Exploring field vegetation reflectance as an indicator of soil contamination in river floodplains. *Environ Pollut* 127(2):281–290. doi:[10.1016/S0269-7491\(03\)00266-5](https://doi.org/10.1016/S0269-7491(03)00266-5)
- Leprieur C, Kerr YH, Mastorchio S, Meunier JC (2000) Monitoring vegetation cover across semi-arid regions: comparison of remote observations from various scales. *Int J Remote Sens* 21:281–300
- Lévesque J, King DJ (2003) Spatial analysis of radiometric fractions from high-resolution multispectral imagery for modelling individual tree crown and forest canopy structure and health. *Remote Sens Environ* 84(4):589–602. doi:[10.1016/S0034-4257\(02\)00182-7](https://doi.org/10.1016/S0034-4257(02)00182-7)
- Lewis M, Jooste V, de Gasparis AA (2001) Discrimination of arid vegetation with airborne multispectral scanner hyperspectral imagery. *IEEE T Geosci Remote* 39(7):1471–1479. doi:[10.1109/36.934078](https://doi.org/10.1109/36.934078)
- Li QT (2006) The extraction and analysis of remote sensing biogeochemistry effects of vegetation in dexing copper mine area. Dissertation, Shandong University of Science and Technology
- Li DC, Xu BB, Shi XR (1996) Influence of simulated acid rain on characteristics of reflectance spectra of rice leaves. *Remote Sens Environ China* 11(4):241–247. doi:[CNKI:SUN:YGXB.0.1996-04-000](https://doi.org/CNKI:SUN:YGXB.0.1996-04-000)
- Li L, Ustin L, Lay M (2005) Application of AVIRIS data in detection of oil-induced vegetation stress and cover change at Jornada, New Mexico. *Remote Sens Environ* 94:1–16. doi:[10.1016/j.rse.2004.08.010](https://doi.org/10.1016/j.rse.2004.08.010)
- Li QT, Yang FJ, Zhang B, Zhang X, Zhou GZ (2008) Biogeochemistry responses and spectral characteristics of *Rhus Chinensis* Mill under heavy metal contamination stress. *J Remote Sens* 12(2):284–290
- Liu SW, Gan FP, Wang RS (2004) The application of Hyperion data to extracting contamination information of vegetation in the DeXing copper mine, Jiangxi Province, China. *Remote Sens Land Resour* 1:6–10
- Ludwig JA, Bastin GN, Chewings VH, Eager RW, Liedloff AC (2007) Leakiness: a new index for monitoring the health of arid and semiarid landscapes using remotely sensed vegetation cover and elevation data. *Ecol Indic* 7:442–454. doi:[10.1016/j.ecolind.2006.05.001](https://doi.org/10.1016/j.ecolind.2006.05.001)
- Muller G, Tang H (1996) Ecological effects of heavy-metal pollution in the Dexing copper mine region in JiangXi Province, China. Final report of the Co-operative Ecological Research Project (CERP). United Nations Educational, Scientific and Cultural Organization, Paris
- Noland TL, Miller JR, Moorthy I, Panigada C, Zarco-Tejada PJ, Mohammed GH et al (2003) Bioindicators of forest sustainability: Using remote sensing to monitor forest condition. In: Buse LJ, Perera AH (eds) Meeting emerging ecological, economic, and social challenges in the Great Lakes region: Popular summaries. Ontario Forest Research Institute, Ontario Ministry of Natural Resources, Forest Research Information 155:75–77
- Pearlman JS, Barry PS, Segal CC, Shepanski J, Beiso D, Carman SL (2003) Hyperion, a space-based imaging spectrometer. *IEEE Trans Geosci Remote Sens* 41(6):1160–1173. doi:[10.1109/TGRS.2003.815018](https://doi.org/10.1109/TGRS.2003.815018)
- Raymond OL (1996) Pyrite composition and ore genesis in the Prince Lyell copper deposit, Mt Lyell mineral field, western Tasmania, Australia. *Ore Geol Rev* 10:231–250. doi:[10.1016/0169-1368\(95\)00025-9](https://doi.org/10.1016/0169-1368(95)00025-9)
- Rosso PH, Pushnik JC, Lay M, Ustin SL (2005) Reflectance properties and physiological responses of *Salicornia virginica* to heavy metal and petroleum contamination. *Environ Pollut* 137(2):241–252. doi:[10.1016/j.envpol.2005.02.025](https://doi.org/10.1016/j.envpol.2005.02.025)
- Sampson PH, Zarco-Tejada PJ, Mohammed GH, Miller JR, Noland TL (2003) Hyperspectral remote sensing of forest condition: estimating chlorophyll content in tolerant hardwoods. *For Sci* 49(3):381–391

- Schuenger AC, Capelle GA, Di Benedetto JA, Mao C, Thai CN, Evans MD, Richards JT, Blank TA, Stryjewski EC (2003) Comparison of two hyperspectral imaging and two laser-induced fluorescence instruments for the detection of zinc stress and chlorophyll concentration in bahia grass (*Paspalum notatum* Flugge). *Remote Sens Environ* 84:572–588. doi:[10.1016/S0034-4257\(02\)00181-5](https://doi.org/10.1016/S0034-4257(02)00181-5)
- Serrano L, Penuelas J, Ustin SL (2002) Remote sensing of nitrogen and lignin in Mediterranean vegetation from AVIRIS data: decomposing biochemical from structural signals. *Remote Sens Environ* 81:355–364
- Shi W, Bischoff M, Turco R, Konopka A (2002) Long-term effects of chromium and lead upon the activity of soil microbial communities. *Appl Soil Ecol* 21:169–177. doi:[10.1016/S0929-1393\(02\)00062-8](https://doi.org/10.1016/S0929-1393(02)00062-8)
- Sims DA, Gamon JA (2003) Estimation of vegetation water content and photosynthetic tissue area from spectral reflectance: a comparison of indices based on liquid water and chlorophyll absorption features. *Remote Sens Environ* 84:526–537. doi:[10.1016/S0034-4257\(02\)00151-7](https://doi.org/10.1016/S0034-4257(02)00151-7)
- Stauber JL, Benning RJ, Hales LT, Eriksen R, Nowak B (2000) Copper bioavailability and amelioration of toxicity in Macquarie Harbour, Tasmania, Australia. *Mar Freshw Res* 51:1–10. doi:[10.1071/MF99010](https://doi.org/10.1071/MF99010)
- Steven MD, Malthus TJ, Baret F, Xu H, Chopping MJ (2003) Intercalibration of vegetation indices from different sensor systems. *Remote Sens Environ* 88:412–422. doi:[10.1016/j.rse.2003.08.010](https://doi.org/10.1016/j.rse.2003.08.010)
- Ustin SL, Smith MO, Jacquemoud S, Verstraete MM, Govaerts Y (1999) Geobotany: vegetation mapping for earth sciences. In: Rencz AN (ed) *Remote sensing for the earth sciences: manual of remote sensing*, vol 3. New John Wiley, New York, pp 189–248
- Xu R, Ma Y, He Z (2003) *Remote sensing in biogeochemistry*. Guangdong Science and Technology Press, Guangzhou
- Yoder BJ, Waring RH (1994) The normalized difference vegetation index of small Douglas-fir canopies with varying chlorophyll concentrations. *Remote Sens Environ* 49:81–91. doi:[10.1016/0034-4257\(94\)90061-2](https://doi.org/10.1016/0034-4257(94)90061-2)
- Zarco-Tejada PJ, Miller JR, Harron J, Hu B, Noland TL, Goel N et al (2004a) Needle chlorophyll content estimation through model inversion using hyperspectral data from boreal conifer forest canopies. *Remote Sens Environ* 89:189–199. doi:[10.1016/j.rse.2002.06.002](https://doi.org/10.1016/j.rse.2002.06.002)
- Zarco-Tejada PJ, Miller JR, Morales A, Berjón A, Agüera J (2004b) Hyperspectral indices and model simulation for chlorophyll estimation in open-canopy tree crops. *Remote Sens Environ* 90(4):463–476. doi:[10.1016/j.rse.2004.01.017](https://doi.org/10.1016/j.rse.2004.01.017)
- Zhang Y, Chen JM, Miller JR, Noland TL (2008) Leaf chlorophyll content retrieval from airborne hyperspectral remote sensing imagery. *Remote Sens Environ* 112:3234–3247. doi:[10.1016/j.rse.2008.04.005](https://doi.org/10.1016/j.rse.2008.04.005)